Applied Nanoscience (2018) 8:1629–1640
https://doi.org/10.1007/s13204-018-0850-5

ORIGINAL ARTICLE

Tolnaftate–graphene composite-loaded nanoengineered electrospun scaffolds as efficient therapeutic dressing material for regimen of dermatomycosis

Shashi Kiran Misra[1] · Pramod W. Ramteke[1] · Sandip Patil[2] · Avinash C. Pandey[3] · Himanshu Pandey[1]

Received: 6 June 2017 / Accepted: 31 July 2018 / Published online: 11 August 2018

Abstract

Graphene "The novel carbon nano-trope" tailors auspicious platform for designing antimicrobial regimen by virtue of its conspicuous molecular interaction with the microorganism. In this work, Tolnaftate (Tf), an antifungal drug, was mingled with Graphene nanoplatelets (Gn) to develop composite (Tf–Gn) via the wet chemical route, embedded in a biocompatible polymeric blend of Eudragit RL100/Eudragit RS100 (EuRL100/EuRS100) and subjected to electrospinning to obtain nonwoven nanoengineered scaffolds (nanofibers) for enhanced anti-dermatophytic virtue. Pursuing cluster of optimization experiments, 20% w/v EuRL100/EuRS 100 was found to be adequate for formation of smooth, defect-free, and regular fibers. Field emission electron microscopy (FESEM) acknowledged zestfully fabrication of smooth, shiny, nano-range, and mesh-like architecture, comprising distinct pockets within their structure. Fourier transform infrared spectroscopy (FTIR) and differential scanning calorimeter (DSC) conceded formation of the composite Tf–Gn, its physical compatibility with polymers, and improved thermal behavior. Exceptional swelling capacity, significant hydrophilicity, and immense drug entrapment efficiency were obtained of nanofibers fabricated from 3:1 ratio of EuRL100/EuRS100 polymers blend owing to relatively higher permeability which gratified essential benchmark for fabrication of nanofibrous scaffold to alleviate fungal infections caused by dermatophytes. In vitro drug release interpreted controlled liberation of Tf in dissolution media, following Korsmeyer–Peppas model kinetics, and suggested a diffusion-based mechanism. Microdilution broth method was performed for in vitro antifungal efficacy against extremely devastating dermatophytes, i.e., anthropophilic Trichophyton rubrum and zoophilic Microsporum canis, exhibited preeminent growth inhibition against T.rubrum and scanty for M.canis. Findings revealed the superior antifungal activity of Tf–Gn-loaded nanofibers as compared to Tf-loaded nanofibers and recommended potential dressing materials for an effective regimen of dermatomycosis.

Keywords Graphene · Tolnaftate · Composite · Dermatomycosis · Dressing materials

Introduction

From the last decade, Graphene has been widely resorted to biomedicine and health services to control delivery of bioactive agents and gene/DNA for therapeutic purposes (Ryoo et al. 2010; Liao et al. 2011; Mendes 2013). Architecturally, graphene, a monolayer of tightly packed carbon atoms (Geim and Novoselov 2007; Wang et al. 2014), possesses multiple attachment sites (Kakran and Li 2012; Kim and Kim 2012) and tremendous surface area (Qin et al. 2014) also portrays vital podium to conspicuous molecular interaction with microorganism (Shen et al. 2012; Zou et al. 2016). Exceptionally immense surface to volume scale (Sur 2012; Drieschner et al. 2016; Qian et al. 2014) and smaller dimension than cells and cellular organelles (Zhang et al. 2016;

✉ Himanshu Pandey
himanshu.nac@gmail.com

[1] Department of Pharmaceutical Sciences, Sam Higginbottom University of Agriculture, Technology and Sciences, Allahabad, India

[2] E-Spin NanoTech Private Ltd., SIDBI Innovation & Incubation Center, Indian Institute of Technology, Kanpur 208016, India

[3] Nanotechnology Application Centre, Institute of Interdisciplinary Studies, University of Allahabad, Allahabad 211002, India

Snitka 2015) expedite graphene to permeate into basic biological structures (Cherian and Mohanan 2014; McCallion et al. 2016) and disruption of cell functions of microorganisms (Roda et al. 2014; Liu et al. 2011a). The enormous loading of the bioactive agent onto the surface of graphene sheets (Akhavan and Ghaderi 2010; Liu et al. 2011b) tailors promising nanoplatforms for designing antimicrobial dosage formulations. Moreover, our research group Pandey et al. (2011) investigated the enhanced antibacterial property of graphene-loaded gentamicin to eradicate gram-negative bacteria causing topical infection (Pandey et al. 2011).

Dermatomycosis caused by topical fungi or dermatophytes positioned as 4th of most common disease in the last decade and affected 20–25% world's population (Peres et al. 2010; Sharma et al. 2015). In an opportunistic role, they are extremely devastating, as these bugs take advantage of a host with the weakened immune system (Araujo et al. 2009). Morphologically dermatophytes are filamentous (Sharma and Sharma 2010), keratinophilic (Lakshmipathy and Kannabiran 2010), mortifying and comprise anamorphic genera of *Microsporum, Trichophyton*, and *Epidermophyton* species (Nosanchuk 2006; Kaufman et al. 2007). Essentially they secrete a proteolytic enzyme, affect keratin by utilizing keratinous substrates (carbon, nitrogen, and sulfur), and make environment alkaline at the infection site (Rossi et al. 2012; Majeed et al. 2016). Although there is a huge inventory of conventional antidermatophytes and antibiotics in the market, they are effective as prophylactic at prelim stage, (Akhtar et al. 2015) but at the advanced state of infection, these measures prove rather helpless due to some shortcomings associated with the type of dosage formulations. Moreover, their indiscriminate and prolonged massive doses mostly cause disease recurrence up to 20–40% (Woodfolk 2005), resistance (Dias et al. 2013), and patient discomfort by causing adverse effects. Furthermore, the regimen also triggers on host's immune system and create allergic symptoms like itching or burning sensations in the host.

Thiocarbamate derivative Tolnaftate (Tf) is selected as the model drug, as it inhibits squalene epoxidase an enzyme, accumulates squalene, and hence causes a deficiency of ergosterol in the cell walls of dermatophytes (Yamaguchi et al. 2001; Kuzetyte and Drevinskas 2011). It is marketed as gel, cream, and aerosol spray with shortcomings of poor efficacy, stickiness, and irritation at the site of application, which leads to lengthening of the therapy time. Thus, minimizing these flaws through designing efficient tolnaftate dosage formulation against dermatophytes with adequate patient compliance and minimize chances of recurrence is one of the objectives of the present study.

A perusal of relevant literature reveals that structurally organized, nonwoven, and therapeutically active 3D nanofibers (Dhivya et al. 2015; Sill and Von 2008) mimic the natural niche of the cells and display endless role in tissue engineering (Lin et al. 2012), regeneration of cell growth (Khil et al. 2003), and cell proliferation (Manea et al. 2016; Tian et al. 2015) by virtue of their marked surface area (Vasita and Katti 2006; Subbiah et al. 2005), pronounced mechanical support (Huang et al. 2004; Tan and Lim 2006), and mesh-like network (Wu et al. 2015; Park et al. 2016). The ability to upload numerous bioactive compounds (Lin et al. 2012; Xiao et al. 2010) into ultrafine fibrous architecture increases their potential for topical dressing materials and scaffolds (Nagesh et al. 2014; Abbaspour et al. 2015). An added attribute of such formulation is its localized nature of effective arena of the drug that interacts with the pathogen (Ulubayram et al. 2015). It strictly follows a confinement and does not allow any drug escalation into surrounding areas to create any drug interaction with the healthy host tissue.

Polymethacrylate polymers (Eudragit RL 100 and Eudragit RS 100) have been selected for fabrication of nanofibrous scaffold due to their inherent properties such as efficient adhesion (Bucolo et al. 2002; Pendekal and Tegginamate 2012) and biocompatibility (Pignatello et al. 2002a, b) with classiness (Pignatello et al. 2002) over the skin surface. By virtue of their variable permeable property, a customized proportion of both polymers for controlled drug release from the nanofibrous scaffold is studied in the present work. We herein explored topical antifungal property of graphene by fabricating tolnaftate–graphene (Tf–Gn) composite-loaded eudragit scaffolds and check out its in vitro competence against mortifying dermatophytes.

Materials and method

Graphene nanoplatelets (Gn) were purchased from Reinste Pvt. Ltd, India. Biocompatible Eudragit RL100 (EuRL 100) and Eudragit RS100 (EuRS 100) polymers of molecular weight 150,000 Da were procured as gift sample from Evonik (Rohm Pharma, Darmstadt, Germany). Tolnaftate (Tf) was received from Belco Pharmaceuticals, India. Dermatophyte strains, i.e., *T.rubrum* (MTCC 7859) and *M.canis* (MTCC 2820) were procured from Microbial Type Culture Collection (MTCC), Chandigarh, India. Polyethylene glycol (PEG 400), RPMI 1640 (Roswell Park Memorial Institute Medium) and MOPS (morpholinepropanesulfonic Acid) were purchased from Sigma-Aldrich Chemicals Pvt. Ltd, India. Sabouraud Dextrose Agar (SDA) was purchased from HiMedia Laboratories Pvt. Ltd, Mumbai, India. Methanol (MeOH), N, N-Dimethylacetamide (DMAc), and Dimethyl sulfoxide (DMSO) were of analytical grade and procured from Merck, India.

Development of composite (Tf–Gn) from tolnaftate and graphene nanoplatelets

Initially, drug tolnaftate (Tf) was loaded efficiently on the graphene nanoplatelets (Gn) through wet chemical route to get composite of tolnaftate–graphene nanoplatelets (Tf–Gn). Briefly, Tf (1 mg/ml) was loaded onto the uniform dispersion of Gn in acetone, and subjected to sonication for few seconds. The resultant dispersion was stirred overnight at room temperature in dark and was ultracentrifuged at 15,000 rpm for 30 min. Conclusively loading capacity of Tf was determined by measuring the concentration of the unbound Tf present in the supernatant using UV–visible spectrophotometer (Shimadzu, 1700) by executing straight line equation ($y = 0.0606 + 0.0075$).

Optimization of the concentration of blend of EuRL100/EuRS100 polymers for fabrication of nanofibers

An equal ratio of 5, 10, 15, and 20% w/v EuRL100 and EuRS100 granules were dissolved in the solvent blend of MeOH and DMAc (4:1). All the mixtures were stirred at room temperature for 12 h with a magnetic stirrer (Corning, Inc., MA, USA) to ensure complete dissolution of the granules of polymers and to obtain homogeneous solutions. The prepared solutions were left to rest for 1 h for degassing and kept in sealed containers at room temperature. 1% v/v PEG 400 was added to provide sufficient flexibility and mechanical strength to the fabricated fibers (Frusawa et al. 2003). Finally, homogenous polymeric solution (EuRL 100/EuRS 100) was processed for electrospinning (E-Spin, Nanotech) to fabricate nanofibers. The prepared polymeric solution was loaded into 10-ml plastic syringe of 15 mm diameter equipped with a sharp needle. The air was manually removed from the needle by pushing the polymer solution through the syringe until it emerged at the end of the needle. The syringe was placed in a syringe pump and the needle was connected to a high-voltage supply. Flow rate from needle was modulated at 5 µl/min, connected to a 15-kV positive power supply (Gamma High Voltage Research, Inc.) from distance of 12 cm at room temperature, 37% relative humidity and directed at a grounded, 80-mm-diameter circular, brass collector (Wang et al. 2009).

Fabrication of EuRL 100: EuRS 100 nanofibers embedded with drug Tf and composite Tf- Gn

Furthermore, individually Tf and Tf–Gn each 1% w/v were loaded to different ratios of (1:3, 1:1, and 3:1) EuRL100: EuRS 100 polymeric solution. The prepared dispersion was mixed with 1% v/v PEG 400 and subjected to the process of electrospinning considering above process parameters. As the voltage was increased, the repulsive electrical force pulled the pendant drop into a conical shape acknowledged as Taylor Cone, and when the electrical force overcomes the surface tension, a liquid jet emerged from the syringe (Zargham et al. 2012), which reaches the bras collector in the form of fine fibers within nanoseconds.

Characterization: Fourier Transform Infrared (FTIR) Spectroscopy

The local compositional and chemical characteristics of the samples were evaluated by FTIR spectroscopy measurements on FTIR-ATR, Bruker Optik, Gmbh, Germany consisting of a DLaTGS detector with a germanium internal reflection element (IRE) crystal. Measurements were performed on the individual physical mixture, Tf, Gn, developed composite, Tf-loaded nanofibers, and Tf–Gn-loaded nanofibers at wave numbers ranging from 4000 to 500 cm^{-1}.

Differential scanning calorimetry

Differential scanning calorimetry (DSC) is a thermoanalytical technique that monitors heat effects associated with phase transitions, chemical reactions as a function of temperature, and thermal transitions relating energy or heat capacity changes, such as melting, glass transitions, recrystallization, and mesomorphic transition temperature. DSC was performed through Thermogravimetric/Differential Thermal Analyzer (Perkin–Elmer, Pyris Diamond TG/DTA). Data were treated mathematically using the resident Pyris Software. Approximately 5 mg of samples (physical mixture, Tf, Gn, Tf–Gn, and their nanofibers) was heated from 25 to 800 °C with a heating rate of 10°C/min.

Surface topography

The surface topography of the fabricated nonwoven electrospun nanofibers was investigated with Field Emission Scanning Electron Microscopy (FESEM quanta 200, Zeiss, Germany). The samples were sputter-coated with gold for better conductivity during imaging. Average fiber diameter and fibers distribution were measured using Adobe Acrobat 9 Pro software.

The static water contact angle (WCA) was analyzed to describe the extent of hydrophilicity through sessile drop method (Siddiqui et al. 2017) using Rame-Hart contact angle goniometer equipped with video capture at room temperature. The amount of 30 µL of deionized water was dropped onto a dried electrospun nanofiber (2 cm^2) with a microsyringe in an atmosphere of saturated water vapor and WCA was estimated after 60 s of incubation time to avoid any deviation. Five different contact angles were averaged to get a reliable value.

Swelling index is considered as an important tool for estimation of drug release behavior from the nanofibrous scaffold, carried out in skin pH 6.8 by gravimetric method (Choi et al. 2010). Each fabricated nanofibrous scaffold (2 cm^2) was kept in Petri plate containing 10 ml media and incubated for 24 h at 37 °C. Then the media adhered on the scaffold surface were removed with filter paper and weighed in a wet condition until constant weight was obtained. The average degree of the swelling index was measured by three successive observations of each nanofiber.

In vitro drug release studies

The release characteristic of drug Tf from electrospun nanofibrous scaffolds was analyzed by dialysis bag method (Shen et al. 2013), maintained at a constant temperature (37 ± 0.5 °C) under mixing conditions using a magnetic stirrer. Dialysis was done by using HIMEDIA® LA 387 Dialysis Membrane-50 having the pore size of 2.4 nm and molecular weight (12,000–14,000 Dalton) against various release mediums, maintaining the sink condition. The interference studies were also done prior to in vitro dissolution studies in order to ensure that the selected polymers did not show interaction with the analysis of drug.

During fungal infection, acidic pH of skin drastically changes towards alkaline region (Panther and Jacob 2014), and hence drug release from fabricated nanofibers was studied and compared in different release mediums, acetate phthalate buffer pH 3.8, phosphate buffer pH 6.8, and alkaline borate buffer pH 9.0. The individually sealed dialysis bag (5 cm) containing Tf and composite Tf–Gn nanofibers equivalent to 1 mg Tf was placed in 200 mL of the abovecited release mediums, stirred at 100 rpm to prevent the formation of a stagnant layer at the bulk and outer solution interface. The aliquots were withdrawn from each medium after every 30 min and replaced with the same fresh dissolution medium, maintaining the sink condition. Tf present in the withdrawn aliquots was quantified by UV spectrophotometer at λmax 258 nm. The drug release assay was performed in triplicate, and average values were narrated using straight line equation.

Furthermore, in order to understand the in vitro release kinetics of drug Tf from the both fabricated nanofibers, four most applied mathematical models (zero order model, first-order model, Higuchi square root model, and Korsmeyer–Peppas model) were applied (Table 1).

In vitro antifungal activity through broth microdilution method

The broth microdilution assay was executed to quantify inhibitory concentration towards dermatomycosis following Clinical and Laboratory Standards Institute guidelines (CLSI). Overnight cultivated fungal strains were suspended in Roswell Park Memorial Institute Medium (RPMI 1640) supplemented with L-glutamine and 2% glucose buffered to pH 7 with 0.165 mol/L morpholinepropanesulfonic acid (MOPS) to yield 1×10^5 CFU/mL in a sterile flat-bottomed 96-well microtiter plate.

An inoculum suspension of the two selected dermatomycosis, i.e., *Trichophyton rubrum* (MTCC 7859) and *Microsporum canis* (MTCC 2820), was prepared, following the National Committee for Clinical Laboratory Standards (NCCLS) guidelines. One-week-old dermatophytes were both subcultured onto sabouraud dextrose agar (SDA) plates at 30 °C and stock inoculum suspensions were made in 10 ml of dimethyl sulfoxide (DMSO) by gently probing the surface with the tip of a Pasteur pipette. The resulting mixtures of spores and hyphal fragments were withdrawn and transferred to a sterile tube. Heavy particles were allowed to settle for 20 min and the upper homogeneous suspensions were subjected to the vortex. The optical densities of these stock suspensions were adjusted with a spectrophotometer (SPECTRAMAX plus 384, Molecular device, USA) at a wavelength of 530 nm and the turbidity was compared with the 0.5 McFarland to yield the fungal suspension of $1–5 \times 10^5$ cells/ml (Riau et al. 2015). Test samples (fabricated nanofibrous scaffolds each 25 mg/ml) were suspended in DMSO and their serial dilution was carried out to give a final concentration of 0.01–1.25 mg/mL. Percentage growth inhibition against time was assessed by monitoring

Table 1 Comparative correlation coefficient (r^2) calculated after applying different mathematical models

Nanofibers	Zero order			First order			Higuchi			Korsmeyer–peppas		
	pH 6.8	pH3.8	pH9	pH 6.8	pH3.8	pH9	pH 6.8	pH3.8	pH9	pH 6.8	pH3.8	pH9
D1	0.8796	0.7870	0.5262	0.9548	0.8427	0.6266	0.9315	0.8411	0.9278	0.9682	0.8750	0.9328
D2	0.5882	0.6138	0.7043	0.8075	0.7464	0.7995	0.8975	0.8976	0.9269	0.8975	0.8978	0.9305
D3	0.6641	0.6060	0.8171	0.9671	0.7569	0.8863	0.9153	0.9025	0.9155	0.9168	0.9025	0.9388
C1	0.6670	0.6332	0.7745	0.8644	0.8114	0.8319	0.9374	0.9528	0.9393	0.9380	0.9528	0.9396
C2	0.5092	0.6232	0.6899	0.8415	0.8080	0.7858	0.9413	0.9313	0.9453	0.9481	0.9313	0.9461
C3	0.6072	0.4227	0.7745	0.9169	0.7992	0.8902	0.9573	0.9245	0.9448	0.9853	0.9846	0.9648

the optical density at 530 nm through spectrophotometer for 96 h at 30 °C without agitation.

Results and discussion

Development of tolnaftate–graphene composite (Tf–Gn)

Graphene nanoplatelets (Gn) offered noncovalent binding with aromatic hydrophobic drug Tf via simple physical adsorption. The rationale behind developing composite with Gn and Tf may be due to hydrogen bonding between their functional groups. Drug loading capacity was estimated through UV spectrophotometer and found 2.568 with the initial Tf concentration of 1 mg/ml. The higher loading capacity may be due to the less steric hindrance effect of the loaded molecule during developing of the composite and would tailor macromolecules harboring biologically active modules to target tissue/cells infected by dermatophytes. Unlike micelles or liposomal drug carriers, developed Tf–Gn composite would not leak bioactive agent on their delivery pathway and avoid adverse effects towards healthy tissue/cells.

Optimization of the polymeric concentration of EuRL100/EuRS 100 for fabrication of nanofibers

Polymeric droplets of an equal blend of EuRL100/EuRS100 solution (5 and 10% w/v) were observed on the collector, while formation of beaded, irregular, and nonuniform nanofibers was visualized as 15% w/v EuRL100/EuRS100 after electrospinning (Fig. 1). Therefore the concentration of polymers was increased up to 20%w/v to obtain regular, beadles, and consistent nanofibrous scaffold.

The spinneret (tip of the syringe) was found to be clogged by taking solvent mixture MeOH:DMAc at 4:1, and beads were detected (Fig. 2a), this may be due to the high volatility of methanol hence solvent composition was customized in composition of 3:2 (Fig. 2b) to avoid phenomenon of clogging at spinneret and for stable Taylor cone (Garg and Bowlin 2011).

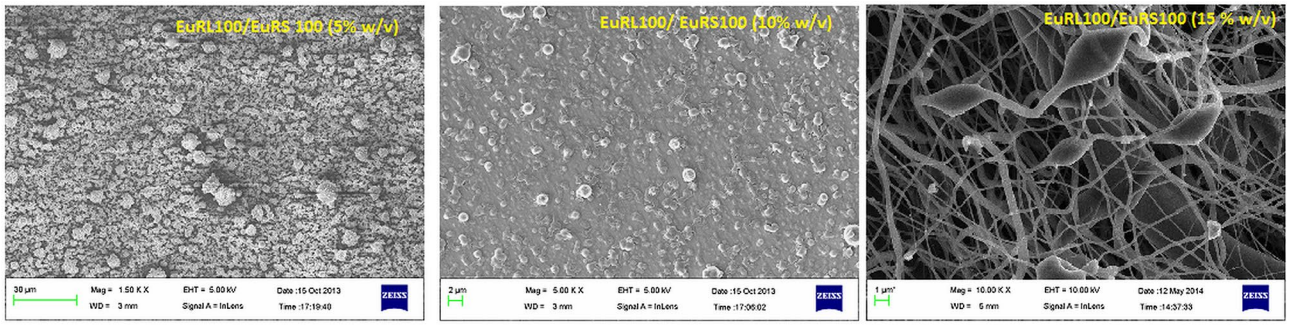

Fig. 1 FESEM of an equal blend of polymers EuRL100/EuRS 100 (5, 10, and 15% w/v) in solvent mixture MeOH: DMAc (4:1)

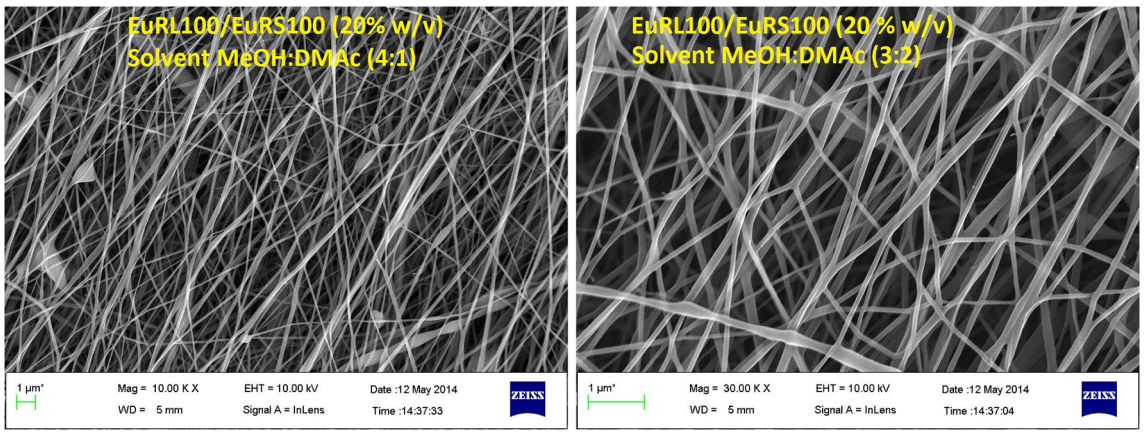

Fig. 2 FESEM of nanofibers fabricated from 20% w/v of an equal blend of EuRL100/EuRS 100 in different solvent compositions MeOH:DMAc (4:1) and (3:2), respectively

Characterization

FTIR spectroscopy

Vibrational analysis of drug Tf revealed C=C stretching mode in the phenyl and naphthalene ring owing to charge transfer interaction between donor and acceptor groups and was responsible for its fungicidal activity (Dhas et al. 2011). The asymmetric C–H stretching mode is being expected approximately at 3095 cm^{-1}, while the symmetric stretching is projected at 2875 cm^{-1}. Figure 3 displays a sharp peak at 1500 cm^{-1} owing to the presence of C–N–C stretching occurred in Tf. It contained meta-disubstituted phenyl ring in its chemical structure that was observed as C=S stretching at 1260 cm^{-1}. Additionally, C–O–C stretching vibration of Tf was seen at 1109 cm^{-1}. In the fingerprint region of Tf-loaded nanofibers, most of the peaks of Tf were shifted, decreased in intensity, or even disappeared. All these were attributed to the hydrogen bonding between the C–O–C group of Tf and the C=O group of EuRL 100/EuRS 100 or the free hydrogen present in quaternary ammonium group of Eudragit. FTIR spectra of Gn showed the presence of different types of O–H stretching vibrations from oxygen functionalities and it was confirmed at 3450 cm^{-1}, whereas C=O stretching vibrations was observed at 1650 cm^{-1}. C–H stretching of CH3 group was observed at 2950 cm^{-1} and C–OH stretching vibrations were present as skeletal vibrations from unoxidized graphitic molecule at 1250 cm^{-1} which were found to be sharp and maybe appeared due to the presence of the remaining carboxyl groups. In the IR spectra of physical mixture, a characteristic band of the C–O–C ester groups at 1110 and 1240 cm^{-1} of EuRL100 and EuRS 100 was observed. The C=O ester vibration was found at 1750 cm^{-1}. Asymmetric CH3 bending of the mixture of polymers was also observed at 1330 cm^{-1}, symmetric CH3 bending showed a peak at 1450 cm^{-1}, and C=O stretching was seen at 1750 cm^{-1}. The presence of quaternary ammonium salt in both polymers EuRL 100 and EuRS 100 showed a prominent peak at 3050 cm^{-1} which were clear from IR spectra. The peaks found to be concordant with functional groups present in the structure of respective polymers. At 3450 and 1650 cm^{-1}, O–H stretching vibrations and C=O stretching, respectively, confirmed the presence of graphene in the physical mixture with no interaction with Tf and polymers.

Vibrational analysis of developed composite Tf–Gn showed the presence of asymmetric C–H stretching mode at 3095 cm^{-1} and the symmetric stretching at 2875 cm^{-1}. Additionally, at 1205 cm^{-1} a peak of C=S stretching and C–N–C stretching appeared at 1507 cm^{-1} indicating the existence of Tf in the developed composite.

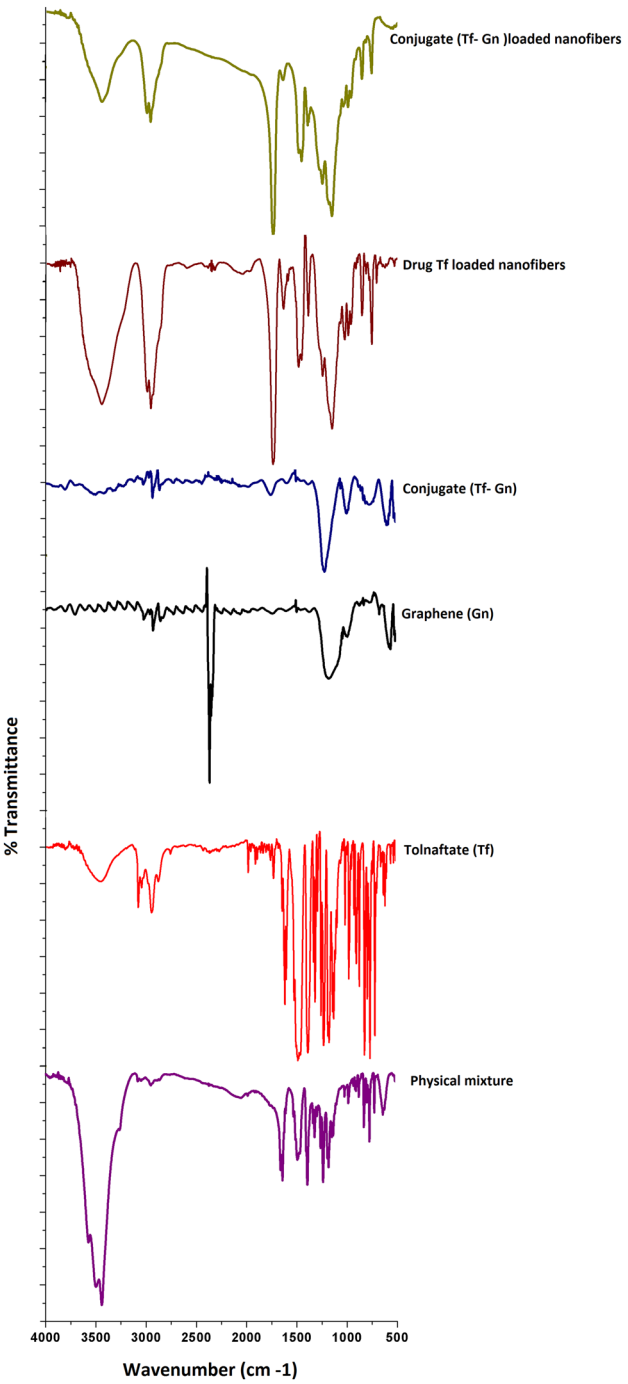

Fig. 3 FTIR analysis of physical mixture, drug Tf, graphene Gn, composite Tf–Gn, Tf-loaded nanofibers and composite (Tf–Gn)-loaded nanofibers

Differential scanning calorimetry (DSC)

Thermal properties or enthalpies of each individual and nanofibers were characterized by differential scanning calorimetry (DSC). A sharp endothermic peak (melting point) of Tf could be seen at 111.23 °C, beside its different peaks

at 162.99, 251.72, 303.28, and 344.72 °C showing polymorphism of drug Tf. Developed composite Tf–Gn showed better thermal stability by virtue of graphene. An endothermic peak at 87.67 °C of the physical mixture showed glass transition temperature of EuRL 100/EuRS 100 polymers, at 350.65 °C degradation of Tf, and a sharp peak at 520.12 °C explained decomposition of Gn present in it. DSC sketch of drug Tf and composite Tf–Gn-loaded nanofibers are compared in Fig. 4b, explaining the better thermal behavior of composite as compared to Tf. The absence of the drug endotherm in fabricated nanofibers indicated the formation of an amorphous dispersion of Tf in the polymeric solution.

Surface topography

Surface topography of Tf-loaded (D, D2, and D3) and Tf–Gn-loaded nanofibrous scaffold analyzed through FESEM revealed an optimized electrospinnability of polymeric (ERL100/ERS100) dispersion with no evident nanoparticles and beads. The FESEM images of D1, D2, and D3 found to be highly branched elongated, regular, and shiny fibers with average diameters of 462.7 ± 40.5, 302.6 ± 50.43, and 402.3 ± 65 nm, respectively. As displayed in Fig. 5, an increased diameter of drug-loaded nanofibers could be attributed to higher drug entrapment or/and improper evaporation of the solvent (MeOH:DMAc) from nanofiber. FESEM of D2 nanofibrous scaffold predicted a smaller size distribution as compared to nanofibers D1 and D3, possibly due to the composition of both EuRL100/EuRS100 (1:1).

By contrast, Fig. 6 compiles FESEM of composite-loaded nanofibrous C1, C2, and C3 scaffolds. They were found to acquire smaller diameter as 229.5 ± 75.23, 105.6 ± 65.3, and 204.5 ± 78.3 nm, respectively, as compare to drug Tf-embedded nanofibers, which explained the enhancement of their surface area. Further uniform distribution of composite in polymeric solution resulted in the smooth surface of the nanofiber with mesh-like appearance, which would be ideal

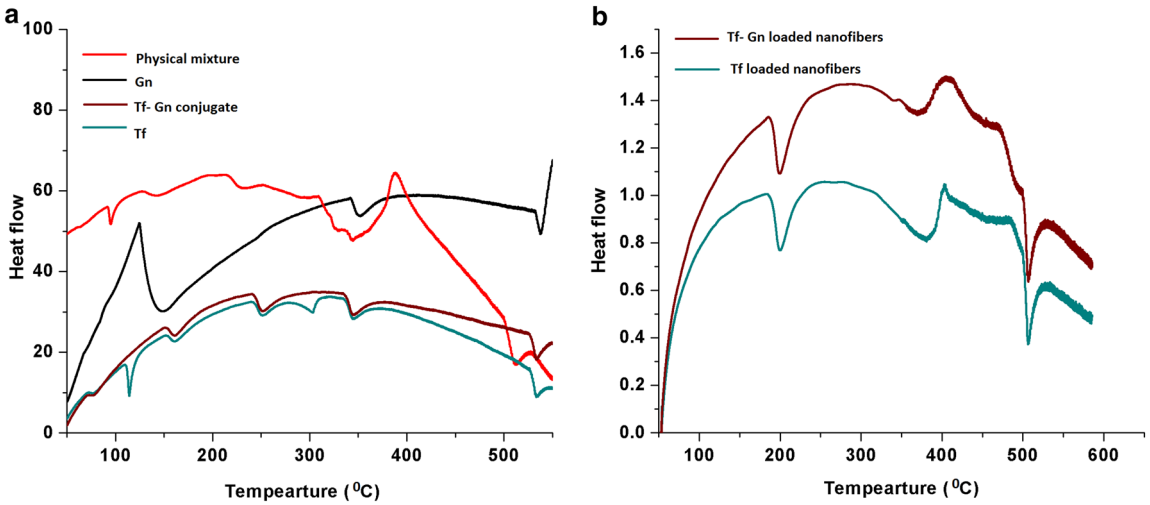

Fig. 4 Compiled DSC of physical mixture, drug Tf, graphene Gn, composite Tf–Gn (**a**), and fabricated nanofibers (**b**)

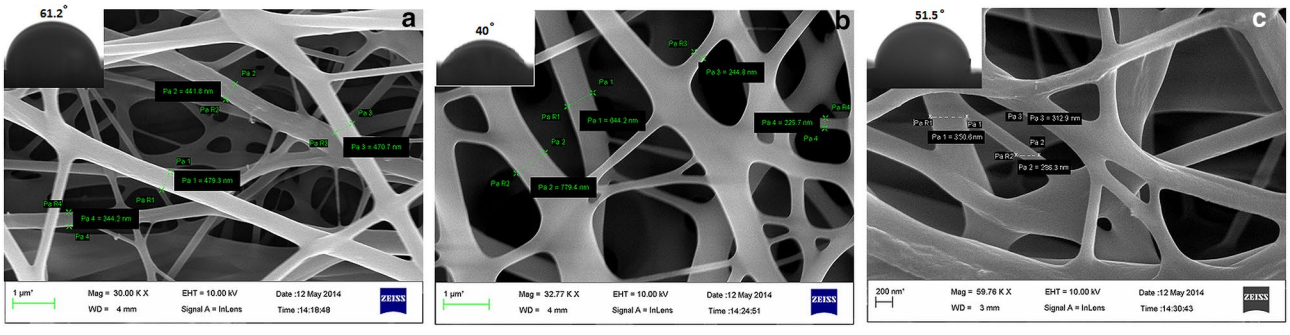

Fig. 5 FESEM observations and particle size distribution. **a** Tf-loaded EuRL100/EuRS100 (D1, 1:3), **b** Tf-loaded EuRL 100/EuRS100 (D2, 1:1), and **c** Tf-loaded EuRL100/EuRS100 (D3, 3:1)

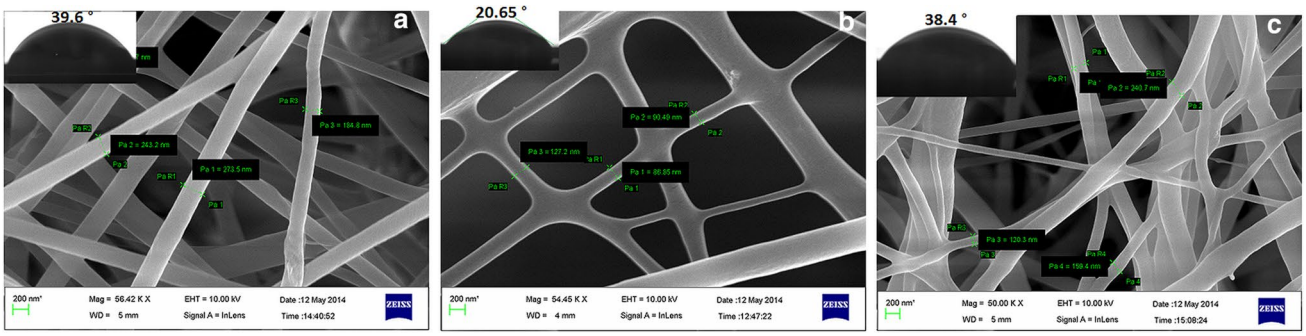

Fig. 6 FESEM observations and particle size distribution. **a** Tf–Gn-loaded EuRL100/EuRS100 (C1, 1:3). **b** Tf–Gn-loaded EuRL 100/EuRS100 (C2, 1:1). **c** Tf–Gn-loaded EuRL100/EuRS100 (C3, 3:1)

criteria for preparation of topical matrix/dressing material for the regimen of dermatomycosis.

Insets of FESEM images of nanofibrous scaffold showed their average water contact angles (WCA). Inherent water permeable property of EuRL100 along with added PEG 400 in polymeric dispersion favored wettability and thus hydrophilic scaffolds were obtained. Least contact angle of C3 nanofibrous scaffold indicated its affinity towards ample exudates produced during dermatophyte infection. Although the existence of numerous voids/pockets on its surface would facilitate spreading of the water droplet and contribute flawless adhesion over the skin and tissue proliferation to a higher extent leading to enhance cure rate, it was also observed that nanofibrous scaffold prepared from the high concentration of EuRS 100 showed maximum water contact angle indicating thicker surface due to possessing the lower amount of quaternary ammonium groups which offered high hydrophobicity.

Figure 7 compares swelling index/capacity of fabricated nanofibrous scaffold after 2, 4, 8, and 24 h. It clearly explored high swelling index of nanofibrous fabricated from polymeric EuRL100/EuRS100 ratio 3:1, i.e., D3 and C3. The presence of higher amount of quaternary ammonium groups in polymer EuRL100 followed by smaller diameter of nanofibers which offered great channels in the form of pockets for absorbing of phosphate buffer pH 6.8 ultimately showed availability of more space for swelling. The degree of swelling decreased after 8 h. The reason behind this could be degradation of integrity of polymeric nanomesh in the medium.

The presence of numerous pockets into its surface architecture might absorb ample of liquid media and thus showed the capability to retain exudates arising during infection.

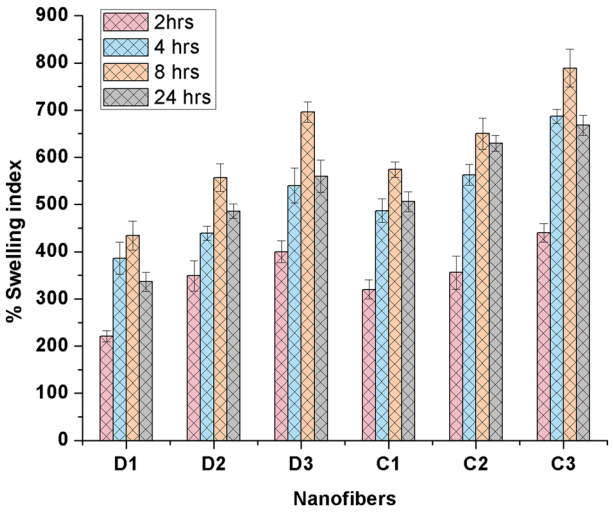

Fig. 7 Compiled swelling index/capacity of Tf-loaded (D1, D2, D3) nanofibers and Tf–Gn-loaded (C1, C2, C3) nanofibers in the different time intervals

Drug loading and drug entrapment efficiency

Drug loading was found to be higher in nanofiber C3 (31.4 ± 4.9%) as compared to nanofibers C1 (20.2 ± 3.8%) and C2 (28.2 ± 2.4%) which attributed to the influence of the higher concentration of EuRL 100 and smaller diameter of nanofibers. It was observed that the entrapment efficiencies of formulations of C1 and C2 were found to be 84.08 ± 5.6 and 88.86 ± 3.6%, respectively, whereas C3 nanofibrous prepared from EuRL100/EuRS100 (3:1) showed the highest entrapment efficiency of 91.92 ± 6.4%. Better entrapment efficacy was attributed to passive drug loading technique which involved the incorporation of the composite into the EuRL 100/EuRS 100 polymeric solution subjected to be spun. This behavior can be explained on the basis of differences in the chemical structures and the percentage content of quaternary ammonium groups. Higher entrapment efficiency would allow significant flexibility to miniature the size of nanofibrous scaffolds for alleviating fungal growth and proliferation at the site.

In vitro drug release

As dermatomycosis alters skin pH from acidic to the alkaline region during their pathogenesis, in vitro study of nanofibrous scaffolds was executed in various dissolution media (acetate phthalate buffer pH 3.8, phosphate buffer pH 6.8, and alkaline borate buffer pH 9.0) to compare and evaluate drug release efficiency. The volume of dissolution medium was kept constant, and the equilibrium between the amount of drug attached to scaffold surface, the fraction dissolved in the buffer, and the amount entrapped in scaffolds is highly controlled by the affinity of the composition of EuRL 100/EuRS 100 polymers. The variable permeability of both polymers justifies the drug release pattern.

In vitro release studies in phosphate buffer pH 6.8 showed that there was an initial burst release of the drug from fabricated nanofibrous scaffold till 2 h followed by controlled release up to 8 h (Fig. 8a). It was observed that higher polymeric concentration of EuRS 100 in nanofiber D1-restricted drug release (19.87 ± 5.92%) up to 2 h in dissolution media owing to its chemical property. By contrast from D3 scaffolds, 39.5 ± 2.81% drug was found to be released in dissolution media attributing higher polymeric concentration of EuRL 100.The maximum percentage cumulative drug release from D3 was estimated 71.5 ± 1.97% after 8 h attributed to the high content of quaternary ammonium compound and facilitated more permeation of dissolution media and hence greater diffusion of the entrapped drug. Similarly, in vitro drug release from composite-loaded nanofibrous C1, C2, and C3 exhibited enhanced drug release concentrations of 50.5 ± 3.41, 61.2 ± 3.43, and 78.5 ± 1.93%, respectively, which must be attributed to enhance release of entrapped drug from the narrow mesh of composite Tf–Gn nanofibrous scaffold. The high surface area and porous structure of the nanofibrous membrane enabled the drugs to diffuse into the dissolution media and to be controlled to release into the medium (El-Newey et al. 2018, Yuri et al. 2011). Moreover, restricted and comparatively less drug release was observed in pH 3.8 (acidic region) and pH 9.0 (alkaline region) from fabricated nanofibers, (Fig. 8b, c, respectively). The drug release behavior from scaffolds was also supported by the swelling studies where the degree of swelling was found to be increased by time, which indicated that the release mechanism is predominantly governed by the diffusion process.

The drug release pattern (initially burst release) explained the presence of a certain amount of drug on the surface of fibers, which was desirable for invading or eradicating dermatophyte prelim stage, and further slow and controlled release of the drug up to 8 h favored antifungal action of nanofibrous scaffold constantly. The presence of PEG 400 might facilitate quick hydration and blend of EuRL100/EuRS100 customized controlled drug release in provided dissolution media. However, drug release from nanofibers was more in phosphate buffer pH 6.8, followed by alkaline borate pH 9.0 and least drug release in acetate buffer pH 3.8 after 8 h, concluding better efficiency on the initial stage of dermatomycosis.

In vitro antifungal activity assay through microdilution broth method

An ideal scaffold/dressing material should be effective to the pathogen and nontoxic to host healthy tissues, and this could be evaluated through in vitro antifungal activity. The antifungal activities of all nanofibrous scaffolds, i.e., P3, D3, G3, and C3, fabricated from the polymeric blend (3:1 EuRL 100: EuRS 100) were examined against selected dermatophytes through broth microdilution method. The purpose was to check the extent of susceptibility of scaffolds with prepared inoculums during the incubation period and also to compare the efficiency of composite-loaded nanofibers C3 with individually drug-loaded D3 and graphene-loaded G3 nanofibers.

Graphs sketched between percentage growth inhibitions and time focused (Fig. 9) showed 98.356% ± 6.34 growth inhibition from C3 against *T. rubrum* for 72 h, after which constant fungicidal effect could be seen up to 96 h that is higher than D3 (91.981% ± 2.67) and G3 (93.652 ± 1.84).

Data obtained also explored the higher susceptibility of nanofibers G3 against *T. rubrum* than D3 which shed

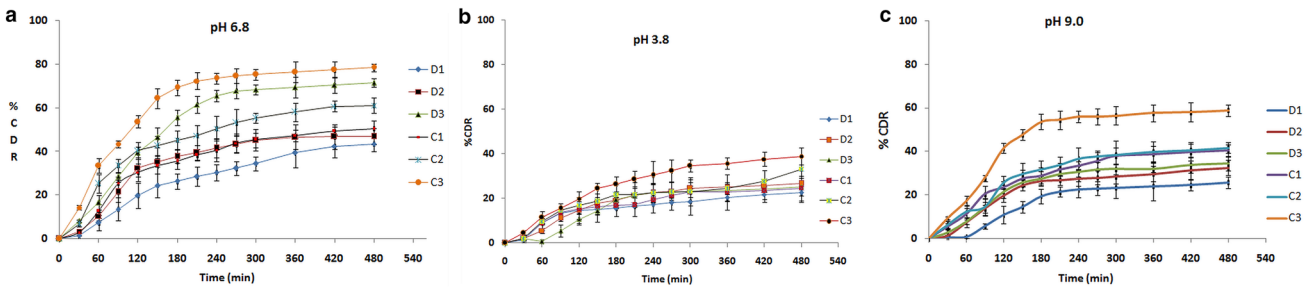

Fig. 8 Comparative drug release from Tf- and Tf–Gn-loaded nanofibers in phosphate buffer pH 6.8, acetate phthalate buffer pH 3.8, and alkaline borate pH 9.0

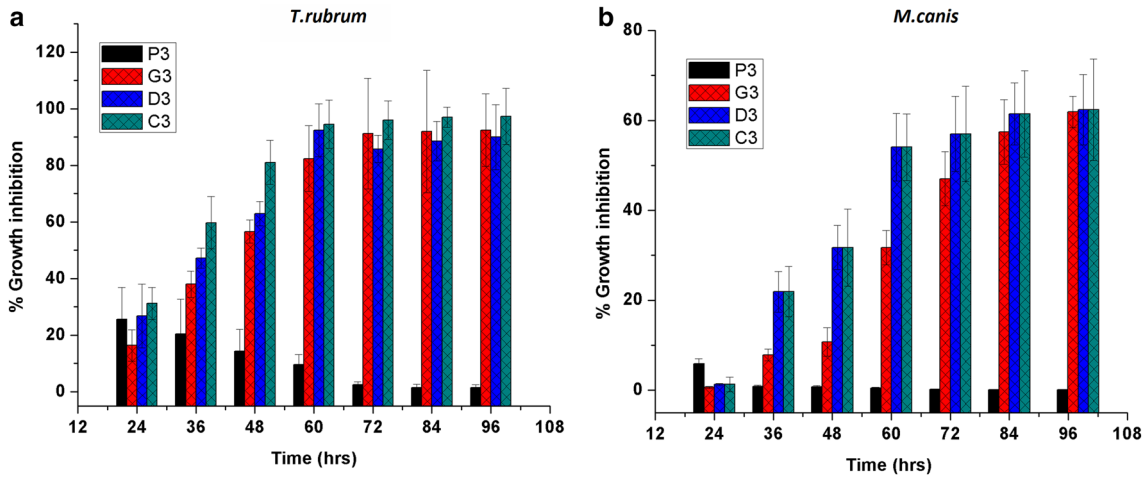

Fig. 9 Comparative % growth inhibition versus time of fabricated nanofibers blank polymeric P3, Gn-loaded G3, drug Tf-loaded D3, and composite Tf–Gn-loaded C3 against *T. rubrum* and *M. canis* (data generated by SoftMax Pro software, model SpectraMax Plus384)

light on the novel application for invading dermatophytes and eradication of nosocomial infections. By contrast, the obtained percentage growth inhibition of *M. canis* was poor and visible fungal colony growth was observed in 96-well microtitre plates during incubation, which suggested its resistant behavior and insufficient concentration of nanofibers for significant antifungal activity.

The findings advocated preeminent antifungal activity towards *T. rubrum*, a causative agent of tinea pedis (athlete's foot), which must be due to an amalgamate action of both Tf and Gn, and also exposed scope for eradication of other 'tinea' diseases that occurred to human as well as animals.

Conclusion

In the present investigation, nanofibrous scaffolds from the variable composition of EuRL100/EuRS100 loaded with tolnaftate Tf, graphene Gn, and its graphene-based composite Tf–Gn were zestfully fabricated. C3 nanofibers, prepared from the polymeric blend of EuRL100/EuRS100 of 3:1 ratio simulated to the extracellular matrix, showed excellent swelling capacity, expedient hydrophilicity, and controlled drug release, which focused on innovative applications for designing dressing materials or bandages to cure dermatomycosis. The drug release pattern (initially burst release) from nanofibers was obtained which was desirable for eradicating dermatophytes at the prelim stage, and further restricted and controlled release of the drug favored antifungal efficiency of nanofibrous scaffold constantly. The findings of micro-broth dilution method advocated superior antifungal activity towards *T. rubrum*, the causative agent of tinea pedis (athlete's foot), which might be due to the combined action of Tf and Gn. Thus, the developed Tf–Gn-loaded nanofibrous scaffold would offer a way to design dressing materials for the treatment of disastrous dermatophytes.

Acknowledgements We thankfully acknowledge the authorities and staff members of Chemical Engineering, IIT Kanpur and Botany Department, the University of Allahabad for generously granting all working facilities and extending their grudgeless cooperation. Our sincere thanks are also for Mr. Akhilesh Kumar Mishra, research scholar, SHUATS, Allahabad for his kind cooperation.

References

Abbaspour M, Makhmalzadeh BS, Rezaee B, Shoia S, Ahangari Z (2015) Evaluation of the antimicrobial effect of chitosan/polyvinyl alcohol electrospun nanofibers containing mafenide acetate. Jundishapur J Microbiol 8(10):e24239

Akhavan O, Ghaderi E (2010) Toxicity of graphene and graphene oxide nanowalls against bacteria. ACS Nano 4:5731–5736

Akhtar N, Verma A, Pathak K (2015) Topical delivery of drugs for the effective treatment of fungal infections of skin. Cur Pharm Desi 21(20):2892–2913

Araujo CR, Miranda KC, Fernandes OFL, Soares AJ, Silva MRR (2009) In vitro susceptibility testing of dermatophytes isolated in Goiania, Brazil, against five antifungal agents by broth microdilution method. Rev Inst Med Trop Sao Paulo 51(1):9–12

Bucolo C, Maltese A, Puglisi G, Pignatello R (2002) Enhanced ocular anti- inflammatory activity of ibuprofen carried by an Eudragit RS 100 nanoparticle suspension. Ophthalmic Res 34(5):319–323

Cherian RS, Mohanan PV (2014) Graphene: a multifaceted nanomaterial for cutting edge biomedical application. Int J Med Nano Res 1:003

Choi J, Lee KM, Wycisk R, Pintauro PN, Mather PT (2010) Nanofiber composite membranes with low equivalent weight perfluorosulfonic acid polymers. J Mater Chem 20:6282–6290

Dhas DA, Joe IH, Roy SD, Balachandran S (2011) Nonplanar property study of antifungal agent tolnaftate-spectroscopic approach. Spectrochim Acta Mol Biomol Spectrosc 79(5):993–1003

Dhivya S, Padma VV, Santhini E (2015) Wound dressings- a review. Biomedicine 5(4):22

Dias MFRG, Filho FB, Santos MVPQ, Amorim AGF, Schechtman RC, Azulay DR (2013) Treatment of superficial mycoses: review—part II. An Bras Dermatol 88(6):937–944

Drieschner S, Weber M, Wohlketzetter J, Vieten J, Makrygiannis E, Blaschke BM, Morandi V, Colombo L, Bonaccorso F, Garrido JA (2016) High surface area graphene foams by chemical vapor deposition. 2D Mater 3(4). iopscience.iop.org/10957-4484/27/3/032001

El-Newehy MH, El-Naggar ME, Alotaiby S (2018) Green electrospinning of hydroxypropyl cellulose nanofibers for drug delivery applications. J Nanosci Nanotechnol 18(2):805–814

Frusawa H, Fukagawa A, Ikeda Y (2003) Aligning a single-lipid nanotube with moderate stiffness. Angew Chem Int Ed Engl 42(1):72–74

Garg K, Bowlin GL (2011) Electrospinning jets and nanofibrous structures. Biomicrofluidics 5(1):013403

Geim AK, Novoselov KS (2007) The rise of graphene. Nat Mater 6:183–191

Huang ZM, Zhang YM, Zhang YZ, Ramakrishna S, Lim CT (2004) Electrospinning and mechanical characterization of gelatin nanofibers. Polymer 12:5361–5368

Kakran M, Li L (2012) Carbon nanomaterials for drug delivery. Key Eng Mater 508:76–80

Kaufman G, Horwitz BA, Duek L, Ullman Y, Berdicevsky I (2007) Infection stages of the dermatophyte pathogen Trichophyton: microscopic characterization and proteolytic enzymes. Med Mycol 45(2):149–155

Khil MS, Cha DI, Kim I, Bhattarai N (2003) Electrospun nanofibrous polyurethane membrane as wound dressing. J Biomed Mater Res 67:675–679

Kim JM, Kim J (2012) Covalent decoration of graphene oxide with dendrimer-encapsulated nanoparticles for universal attachment of multiple nanoparticles on chemically converted graphene. Chem Commun 48:9233–9235

Kuzetyte T, Drevinskas T (2011) Study of tolnaftate release from fatty acids containing ointment and penetration into human skin ex vivo. Acta Poloniae Pharm 68(6):965–973

Lakshmipathy DK, Kannabiran K (2010) Review on dermatomycosis: pathogenesis and treatment. Nat Sci 2(7):726–731

Liao KH, Lin YS, Macosko CW, Haynes CL (2011) Cytotoxicity of graphene oxide and graphene in human erythrocytes and skin fibroblasts. ACS Appl Mater Interfaces 3(7):2607–2615

Lin J, Li C, Zhao Y, Hu J, Zhang LM (2012) Co-electrospun nanofibrous membranes of collagen and zein for wound healing. ACS Appl Mater Interfaces 4(2):1050–1057

Liu S, Zeng TH, Hofmann M, Burcombe E, Wei J et al (2011a) Antibacterial activity of graphite, graphite oxide, graphene oxide, and reduced graphene oxide: membrane and oxidative stress. ACS Nano 5:6971–6980

Liu S, Zeng TH, Hofmann M, Burcombe E, Wie J, Jiang R, Kong J, Chen Y (2011b) Antibacterial activity of graphite, graphite oxide, graphene oxide and reduced graphene oxide: membrane and oxidative stress. ACS Nano 5:6971–6980

Majeed N, Narayanankutty S, Rajan R, Theodore RB (2016) Clinicomycological study of dermatophytosis in a tertiary care centre. J Acad Clin Microbiol 8:110–113

Manea LR, Hristian L, Leon AL, Popa A (2016) Recent advances of basic materials to obtain electrospun polymeric nanofibers for medical applications. IOP Conf Ser Mater Sci Eng 145:032006

McCallion C, Burthem J, Rees-Unwin K, Golovanov A, Pluen A (2016) Graphene in therapeutics delivery: problems, solutions and future opportunities. Eur J Pharm Biopharm 104:235–250

Mendes PM (2013) Cellular nanotechnology: making biological interfaces smarter. Chem Soc Rev 42(24):9207–9218

Nagesh H, Ezzat M, Ghanim M, Hassanin A, El-Moneim AA (2014) Evaluation of antibacterial activity and drug release behavior of chitosan-based nanofibres (in vitro study). UK J Pharm Biosci 2(3):1–5

Nosanchuk JD (2006) Current status and future of antifungal therapy for systemic mycoses. Recent Pat Anti-Infect Drug Discov 1:75–84

Pandey H, Parashar V, Parashar R, Prakash R, Ramteke PW, Pandey AC (2011) Controlled drug release characteristics and enhanced antibacterial effect of graphene nanosheets containing gentamicin sulfate. Nanoscale 3:4104–4108

Panther DJ, Jacob SE (2015) The importance of acidification in atopic eczema: an underexplored avenue for treatment. J Clin Med 5:970–978

Park CH, Bae H, Kwak SJ et al (2016) Interconnection of electrospun nanofibers via a post co-solvent treatment and its open pore size effect on pressure-retarded osmosis performance. Macromol Res 24:314. https://doi.org/10.1007/s13233-016-4044-2

Pendekal SM, Tegginamate PK (2012) Formulation and evaluation of a bioadhesive patch for buccal delivery of tizanidine. Acta Pharm Sin B 2(3):318–324

Peres NT, Maranhao FC, Rossi A, Rossi NM (2010) Dermatophytes: host pathogen interaction and antifungal resistance. An Bras Dermatol 85(5):657–667

Pignatello R, Bucolo C, Puglisi G (2002a) Ocular tolerability of Eudragit RS100® and RL 100 ® nanosuspensions as carriers for ophthalmic controlled drug delivery. J Pharm Sci 16:53–61

Pignatello R, Bucolo C, Ferrara P, Maltese A, Puleo A, Puglisi G (2002b) Eudragit RS 100® nanosuspensions for the ophthalmic controlled delivery of ibuprofen. Eur J Pharm Sci 16:53–61

Qian Y, Ismail IM, Stein A (2014) Ultralight, high-surface-area, multifunctional graphene-based aerogels from self-assembly of graphene oxide and resol. Carbon 68:221–231

Qin Z, Taylor M, Hwang M, Bertoldi K, Buehler MJ (2014) Effect of wrinkles on the surface area: Toward the design of nanoelectronics. Nano Lett 14(11):6520–6525

Riau AK, Mondal D, Aung TT, Murugan E, Chen EL, Lwin NC, Zhou L, Beuerman RW (2015) Collagen-based artificial corneal scaffold with anti-infective capability for prevention of perioperative bacterial infections. ACS Biomater Sci Eng 1:1324–1334

Roda F, Thani A, Patan NK, Mariam A, Maadeed A (2014) Graphene oxide as antimicrobial against two gram-positive and two gram negative bacteria in addition to one fungus. J Biol Sci 14(3):230–239

Rossi NM, Gabriela F, Persinoti GF, Peres NTA, Rossi A (2012) Role of pH in the pathogenesis of dermatophytoses. Mycoses 55:381–387

Ryoo SR, Kim YK, Kim MH, Min DH (2010) Behaviours of NIH-3T3 fibro-blasts on graphene /carbon nanotubes: proliferation, focal adhesion, and gene transfection studies. ACS Nano 4(11):6587–6598

Sharma M, Sharma M (2010) Incidence of dermatophytes and other keratinophilic fungi in the schools and college playground soils of Jaipur, India. Afr J Microbiol Res 4(24):2647–2654

Sharma V, Kumawat TK, Sharma A, Seth R, Chandra S (2015) Distribution and prevalence of dermatophytes in semi- arid region of India. Adv Microbial 5:93–106

Shen J, Burgess DJ (2013) In vitro dissolution testing strategies for nanoparticulate drug delivery systems: Recent developments and challenges. Drug Deliv Transl Res 3(5):409–415

Shen H, Zhang L, Liu M, Zhang Z (2012) Biomedical applications of graphene. Theranostics 2(3):283–294

Siddiqui AR, Maurya R, Balani K (2017) Superhydrophobic self-floating carbon nanofiber coating for efficient gravity-directed oil/water separation. J Mater Chem A 5:2936–2946

Sill TJ, Von RHA (2008) Electrospinning: applications in drug delivery and tissue engineering. Biomaterials 29(13):1989–2006
Snitka V (2015) Graphene based materials: opportunities and challenges in nanomedicine. J Nanomed Res 2(4):00035
Subbiah T, Bhat GS, Tock RW, Parameswaran S, Ramkumar SS (2005) Electrospinning of nanofibers. J Appl Poly Sci 96:557–569
Sur UK (2012) Graphene: a rising star on the horizon of materials science. Int J Electrochem. https://doi.org/10.1155/2012/237689
Tan EPS, Lim CT (2006) Mechanical characterization of nanofibers—a review. Compos Sci Technol 66(9):1102–1111
Tian L, Prabhakaran MP, Ramakrishna S (2015) Strategies for regeneration of components of nervous system: scaffolds, cells and biomolecules. Regen Biomater 2(1):31–45
Ulubayram K, Calamak S, Shahbazi R, Eroglu I (2015) Nanofibers based antibacterial drug design, delivery and applications. Curr Pharm Des 21(15):1930–1943
Vasita R, Katti DS (2006) Nanofibers and their applications in tissue engineering. Int J Nanomed 1:15–30
Wang HS, Fu GD, Li XS (2009) Functional polymeric nanofibers from electrospinning. Recent Patents Nanotechnol 3(1):21–31
Wang X, Sun G, Routh P, Kim DH, Huang W, Chen P (2014) Heteroatom-doped graphene materials: synthesis, properties and application. Chem Soc Rev 4(43):7067–7098
Woodfolk JA (2005) Allergy and dermatophytes. Clin Microbiol Rev 18(1):30–43
Wu N, Wang Y, Lei Y, Wang B, Han C, Gou Y, Shi Q, Fang D (2015) Electrospun interconnected Fe-N/C nanofiber networks as efficient electrocatalysts for oxygen reduction reaction in acidic media. Sci Rep 5:17396. https://doi.org/10.1038/srep17396
Xiao S, Shen M, Ma H, Guo R, Zhu M, Wang S (2010) Fabrication of water- stable electrospun polyacrylic acid-based nanofibrous mats for removal of copper (II) ions in aqueous solution. J Appl Polym Sci 116(4):2409–2417
Yamaguchi H, Uchida K, Tanaka T, Yamaguchi T (2001) Therapeutic efficacy of a topical tolnaftate preparation in guinea pig model of tinea pedis. Jpn J Antibiotics 54(6):323–330
Yuri ML, Pattekari P, Zhang X, Torchilin V (2011) Converting poorly soluble materials into stable aqueous nanocolloids. Langmuir 27(3):1212–1217
Zargham S, Bazgir S, Tavakoli A, Rashidi AS, Damerchely R (2012) The effect of flow rate on morphology and deposition area of electrospun nylon 6 nanofiber. J Eng Fiber Fabr 7(4):42–49
Zhang B, Wei P, Zhou Z, Wei T (2016) Interactions of graphene with mammalian cells: molecular mechanisms and biomedical insights. Adv Drug Deliv Rev 105:145–162
Zou X, Zhang L, Wang Z, Luo Y (2016) Mechanism of the antimicrobial activities of graphene materials. J Am Chem Soc 138(7):2064–2077